ISSN: 2277-3754
ISO 9001:2008 Certified
International Journal of Engineering and Innovative Technology (IJEIT)
Volume 4, Issue 2, August 2014

Flutter and Divergence Characteristics of Composite Plate Wing

M. Kassem Abbas*, Hany M Negm**, M Adnan Elshafei*
* Department of Aeronautics-Military Technical Collage, **Department of Aerospace Engineering-Cairo University, Cairo, Egypt

Abstract: ***In the present work, an analytical investigation is introduced to determine the aero elastic behavior of unswept rectangular wings simulated by cantilevered composite plates using energy formulation and aerodynamic theory for incompressible flow. Modified higher order shear deformation theory (MSDT) is used to formulate the structural deformation. A Doublet point method is used to solve the unsteady subsonic flow over the proposed rectangular wing. The flutter and divergence velocities are obtained using U-g method. Also the effect of composite fiber orientation angles on natural frequency, flutter and divergence speeds are computed. The obtained results are compared with analytical, finite element, wind tunnel test results available in the literature, good agreement is generally found.***

Keywords: **Aero elasticity, Flutter, divergence, composite plate wing, unsteady aerodynamic, doublet point method.**

I. INTRODUCTION

The proposed work is concerned with the aeroelasic behavior of the laminated composite plate wing. The field of aero elasticity involves the mutual interaction among the aerodynamic, inertia, and elastic forces. The wing divergence phenomenon is a static instability of the lifting surface where the inertial forces are neglected, which the flutter phenomena is a dynamic aero elasticity where the inertia force is involved. Several researchers are interested to solve aero-elastic phenomena with different theories. Reference [1] investigated analytical solution with experimental validation of the aero elastic behavior of unswept rectangular wing simulated as graphite/epoxy plates with bending- torsion stiffness coupling. The analytical approach incorporated Rayleigh-Ritz energy formulation and unsteady incompressible two-dimensional aerodynamic theory. Flutter and divergence velocities were obtained using the U-g method and they compared the obtained results to the results of low speed wind tunnel tests. They concluded that wings with negative stiffness coupling exhibit divergence, while the other with positive coupling delayed the occurrence of stall flutter. Reference [2] used 18-degree-of freedom triangular plate finite element. They studied the effects of composite fiber angle, orthotropic modulus ratio, sweep angle, and aspect ratio on the vibration, flutter, and divergence characteristics of cantilever plates in subsonic flow. The stiffness and mass matrices are generated according to the classical lamination theory. The unsteady air load is evaluated using lifting surface theory solved numerically by doublet-lattice method. Interpolation using a surface spline is employed to interconnect the structural nodal and aerodynamic control points. They concluded that effective enhancement of flutter/ divergence performance can be attained by varying the orthotropic modulus ratio when an appropriate fiber orientation is selected. They found also that structural tailoring can provide a harmonious balance to the sweep angle effect upon the aero elastic stability characteristics of a wing. Reference [3] investigated structural damping effect on the flutter boundary for three types of composite wings; rectangular, swept-forward, and swept-back using the finite element technique. The unsteady aerodynamic loads on oscillating wings are evaluated by doublet point method. The interpolation between the structural and aerodynamic grids is accomplished by using surface splines. The effects of fiber orientation on the flutter/ divergence characteristics were investigated. They concluded that the structural damping of composite materials increases the flutter speeds and decreases the flutter frequencies. Reference [4] studied the static and dynamic aero elastic behavior of composite swept wings using a modified approach based on the equivalent plate concept using classical and first order plate theories. He made a parametric study to illustrate the effect of wing aspect ratio, taper ratio, sweep angle, number of layers, and fiber orientations on the divergence, control reversal, and flutter phenomena. He concluded that the wing divergence speed can be improved by moving the principal skin stiffness direction ahead of the wing reference axis. Similarly flutter characteristics of sweep back wings can be improved by moving the principal skin stiffness direction behind the wing reference axis. Reference [5] investigated the nonlinear stalled aero elastic behavior of rectangular graphite/epoxy cantilevered wings with varying amounts of bending-torsion stiffness coupling. A wind-tunnel test was performed to validate the analytical model. Reference [6] used equivalent plate structural modeling and doublet point lifting surface unsteady aerodynamics to obtain analytic sensitivities of aero servo elastic response with respect to wing and control surface plan form shape parameters. He developed an efficient approximation technique for wing shape optimization as a multidisciplinary optimization strategy. Reference [7] presented a theoretical analysis of the flutter suppression of oscillating thin airfoils using active acoustic

ISSN: 2277-3754
ISO 9001:2008 Certified
International Journal of Engineering and Innovative Technology (IJEIT)
Volume 4, Issue 2, August 2014

excitations in incompressible flow. Closed-form unsteady aerodynamic loads induced by a simple harmonic acoustic excitation on a typical section model are derived. The flutter boundaries of the typical section were evaluated using both the U-g and root locus methods. Many methods have been developed for calculating the unsteady pressure distribution on a thin finite wing in subsonic flow. Reference [8] formulated the governing integral equation. The methods can be divided into two principal categories, the mode function method and the direct element method. Reference [9] developed the mode function method for practical use. Reference [10] calculated successfully the unsteady pressure distribution on wings with control surfaces. A typical procedure of the discrete-element method type is the doublet lattice method [11]-[13]. This method is used widely because of its ready applicability to complex wing configurations. Although the method yields reasonable results, it contains an inconsistency in the steady-state part. It must be calculated with the aid of the vortex lattice method despite the fact that the basic equation of doublets is valid even when the flow becomes steady [11]. Reference [14] developed a simple method for calculating unsteady aerodynamic loads on harmonically oscillating thin wings in subsonic flow. Their doublet point method is based on a concept of concentrated lift forces. The wing is divided into element surfaces on which the lift distribution is represented by single concentrated lift forces.

In the present work a modified higher order shear deformation theory (MHSDT) [15] is used to formulate the equation of motion of the composite plate wing. The unsteady aerodynamic loads on harmonically oscillating thin composite plate wings in subsonic flow are calculated. The doublet point method is used based on a concept of concentrated lift forces to solve the subsonic unsteady flow over a rectangular wing. Flutter and divergence velocities are obtained using U-g method and compared to the published analytical, finite element and wind tunnel test results available in the literature and found reasonable.

II. STRUCTURAL FORMULATION

The wing is idealized by a rectangular cantilevered composite plate with uniform thickness. The transverse deflection equation is written in generalized coordinates as follows:

$$w_0(x,y,t) = \{a_3(x,y)\}^T \{q_3(t)\} \quad (1)$$

where $\{a_3(x,y)\}$ is the column vector of the Ritz approximation functions that satisfy the plate boundary conditions and given by [15]:

$$\{a_3(x,y)\}^T = \left[x^2 \;\; x^2y \;\; x^3 \;\; x^2y^2 \;\; x^3y \;\; x^4 \;\; x^3y^2 \;\; x^4y \;\; x^4y^2\right] \quad (2)$$

and $\{q_3(t)\}$ is the unknown column vector of Ritz coefficients. Using Hamilton's principle the equation of motion is obtained and given by [15]:

$$[M]\{\ddot{q}\} + [K]\{q\} = \{F_{z_0}\} \quad (3)$$

where $[K]$ and $[M]$ are the stiffness and mass matrices, $\{F_{z_0}\}$ is the load vector representing the aerodynamic load distribution on the wing which calculated using doublet point method, and $\{q\}$ is the generalized coefficient vector to be determined.

III. UNSTEADY AERODYNAMIC FORMULATION (DOUBLET POINT METHOD)

The doublet point method is used to calculate the subsonic unsteady aerodynamic forces which act on two-dimensional wings. The aerodynamic loads are calculated as concentrated loads vector $\{F_{z_0}\}$. The obtained results by the proposed method can easily be combined with aero elastic analysis to calculate flutter and divergence velocities. The pressure distribution on oscillatory lifting surfaces and its corresponding up-wash velocity distribution are related by the integral equation [8]-[14]-[16]:

$$v_I(x,y) = \frac{1}{8\pi}\iint_S \Delta p(\xi,\eta) K(x_0,y_0)\, d\xi\, d\eta \quad (4)$$

The lifting surface is assumed to lie in the x-y plane (z = 0), where S denotes the region of the wing area and the non-dimensional pressure distribution Δp is defined by:

$$\Delta p = \frac{p_+' - p_-'}{0.5\rho_\infty u_\infty^{\,2}} \quad (5)$$

where p_+' and p_-' are the disturbance pressure on the upper and lower surfaces of the wing, respectively. The denominator on the right-hand side of Eq.(5) is the dynamic pressure of the uniform flow and the Kernel function $K(x_0,y_0)$ in Eq.(5) can be written as:

$$K(x_0,y_0) = e^{-ikx_0}\left[\frac{Me^{ikx}}{R\sqrt{X^2+r^2}} + B(k,r,X)\right] \quad (6)$$

The parameters used in the Eq.(6) are defined in Appendix A [14]. Since the kernel function $K(x_0,y_0)$ corresponds to a normal velocity field that is produced by a point doublet of the acceleration potential located at (ζ,η), it is called a doublet point. The point (x,y) is called an up-wash point where the normal

ISSN: 2277-3754
ISO 9001:2008 Certified
International Journal of Engineering and Innovative Technology (IJEIT)
Volume 4, Issue 2, August 2014

velocity of the up-wash is placed. The wing platform is divided into panel segments called element surfaces. Each element surface is constructed such that the two side edges are parallel to the uniform flow. We identify the individual elements by numbering them from 1 to N as shown in Figure 1.a, and Figure 1.b shows a focus on the i^{th} element surface.

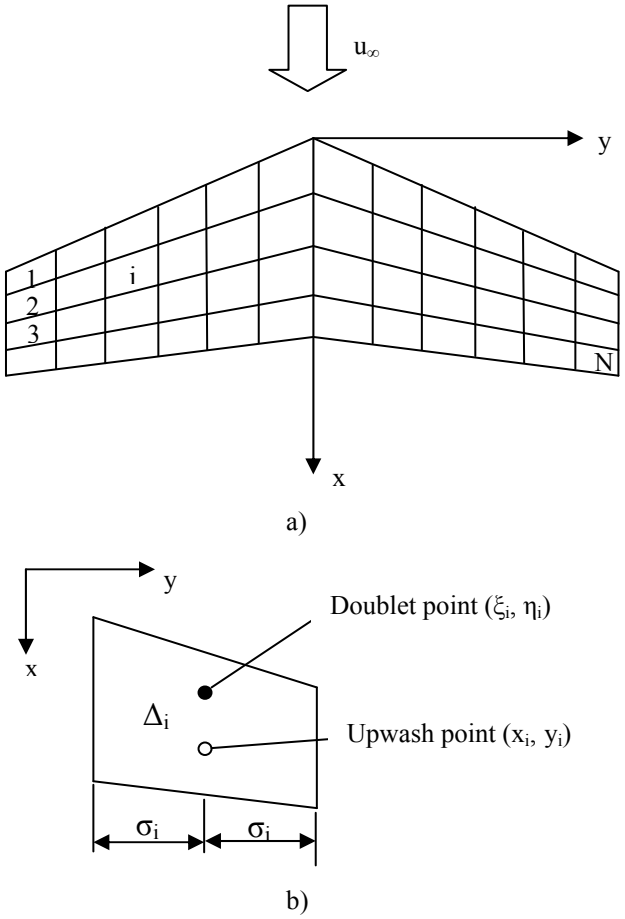

Fig 1. Aerodynamic elements in doublet point method [14].

The trapezoid of the element has an area Δ_i and width $2\sigma_i$. Using (quarter- third quarter chord) rule for element surfaces, the lift distribution on the surface is concentrated at the point (ζ_i, η_i) on the quarter chord at the mid-span of the element i. Thus, the location (ζ_i, η_i) is the doublet point of the element surface i. The up-wash of the three-quarter chord point (x_i, y_i) at the midspan is taken as representative of the whole up wash distribution on the element surface i. These assumptions make it possible to discrete the integral in Eq.(4) into linear algebraic equations. Instead of Eq. (4)the up wash v_i of i^{th} element can be calculated in a discrete form as [14]:

$$v_I(x_i,y_i)=\frac{1}{8\pi}\sum_{j=1}^{N}\Delta p(\xi_j,\eta_j)\Delta_j K(x_i-\xi_j,y_i-\eta_j),\quad (i=1...N) \tag{7}$$

Equation (7) can be expressed in a matrix form as follows:

$$\{v_I\}=[D]\{c_p\} \tag{8}$$

where $\{v_I\}$ is the induced velocities at the element upwash points (x_i, y_i), $[D]$ is the matrix of aerodynamic influence coefficients, and $\{c_p\}$ is the pressure coefficient vector which represents the pressure coefficient at each element's doublet point as shown in Figure 1 and defined as follows:

$$v_I=\{v_{Ii}\}=\{v_I(x_i,y_i)\} \tag{9}$$

$$D=[d_{ij}]=\frac{\Delta_j}{8\pi}K(x_i-\xi_j,y_i-\eta_j) \tag{10}$$

$$c_p=\{c_{p_j}\}=\{\Delta p(\xi_j,\eta_j)\} \tag{11}$$

The upwash vector $\{v_I\}$ is calculated for element i using the following form [14]:

$$v_{I_i}=\frac{\partial}{\partial x}w_0(x_i,y_i)+i\,k\,w_0(x_i,y_i) \tag{12}$$

where $w_0(x_i,y_i)$ is the mid-plane (z=0) vertical displacement at the upwash point (x_i, y_i) of element i. By solving Eq.(8) we can directly obtain the unsteady aerodynamic pressure coefficient distribution at the doublet point of each element area. When the reduced frequency k tends to zero the flow becomes steady. The complex lift and moment coefficients can be calculated as mentioned in Appendix B. Using the transverse deflection equation Eq. (1) the induced velocity can be written as:

$$\begin{aligned} v_{I_i}&=\left([v_{IR}]_i+i\,[v_{II}]_i\right)\{q_3\}\\ [v_{IR}]_i&=\left\{\frac{\partial a_3}{\partial y}(x_i,y_i)\right\}^T\\ [v_{II}]_i&=k\,\{a_3(x_i,y_i)\}^T \end{aligned} \tag{13}$$

The induced velocities of all elements are written in vector form as follows:

$$\begin{aligned} \{v_I\}&=[v_{IT}]\{q_3\}\\ [v_{IT}]&=[v_{IR}]+i\,[v_{II}] \end{aligned} \tag{14}$$

ISSN: 2277-3754
ISO 9001:2008 Certified
International Journal of Engineering and Innovative Technology (IJEIT)
Volume 4, Issue 2, August 2014

where the dimensions of the induced velocity vector $\{v_I\}$ are $N_e \times 1$, and the dimensions of $[v_{IR}]$ and $[v_{II}]$ are $N_e \times 9$, where N_e is the total number of aerodynamic elements. By substituting into Eq.(8), the unsteady aerodynamic pressure coefficient distribution c_p on the plate wing can be written as:

$$\{c_p\} = [D]^{-1}[v_{IT}]\{q_3\} \tag{15}$$

The transverse aerodynamic load at element i can be obtained by:

$$F_{ai} = \frac{1}{2}\rho U^2 S_i c_{p_i} \tag{16}$$

where ρ is the air density, U is the uniform flow speed, and S_i is the area of element i. The transverse load vectors of all elements are given by:

$$\{F_a\} = \frac{1}{2}\rho U^2 [S]\{c_p\} \tag{17}$$

where $[S]$ is a square diagonal matrix consisting of the elements areas. Substituting Eq.(15) into Eq.(17) gives:

$$\{F_a\} = \frac{1}{2}\rho U^2 [Ar]\{q_3\} \tag{18}$$

where $[Ar]$ is a matrix of dimensions $N_e \times 9$ defined as follows:

$$[Ar] = [S][D]^{-1}[v_{IT}] \tag{19}$$

Due to symmetry, the transverse aerodynamic loads applying on the half wing only are taken into consideration. Using the energy method the concentrated load vector in the transverse z-direction applied at the doublet point of element i is given by [15]:

$$\{F_{z_0}\}_i = F_{z_i}\{a_3(\zeta_i, \eta_i)\} \tag{20}$$

where (ζ_i, η_i) is the coordinates of the doublet point of element i as shown in Figure 1 The concentrated load vector in the transverse z-direction applied at the half wing can be written in matrix form as:

$$\{F_{z0}\} = \sum_{i=1}^{N_e/2}\{F_{z0}\}_i = [a_3]\{F_a\} \tag{21}$$

where $[a_3]$ is a matrix of dimensions $9 \times (N_e/2)$ including columns of Ritz approximation functions given in Eq. (2) which is obtained by substituting in column (i) for x and y with ζ_i and η_i of element i from $i = 1$ to $N_e/2$. By inserting $\{F_a\}$, Eq.(18) into Eq. (21) yields:

$$\{F_{z0}\} = \frac{1}{2}\rho U^2 [a_3][Ar]\{q_3\} \tag{22}$$

which represents the form of the transverse load vector applied on the half wing due to unsteady aerodynamics using the doublet point method. It is important to note that the applied aerodynamic load is a function of the column vector of Ritz coefficients $\{q_3(t)\}$ which represents the time-dependent transverse deflection of the mid-plane of the cantilever plate.

Using Eq.(22), the equations of motion of the wing can be written as,

$$[M_w]\{\ddot{q}_3\} + [K_w]\{q_3\} = \frac{1}{2}\rho U^2 [a_3][Ar]\{q_3\} \tag{23}$$

where $[M_w]$ and $[K_w]$ are 9×9 mass and stiffness sub-matrices corresponding to the transverse deflection taken from the global mass and stiffness matrices [15].

IV. FLUTTER ANALYSIS

By assuming harmonic motion $\{q_3(t)\}$ can be expressed as follows:

$$\{q_3\} = \{\bar{q}_3\}e^{i\omega t} \tag{24}$$

Thus;

$$\{\ddot{q}_3\} = -\omega^2\{\bar{q}_3\}e^{i\omega t} \tag{25}$$

where $\{\bar{q}_3\}$ is the amplitude of the column vector of Ritz coefficients, ω is the oscillation frequency. The reduced frequency k is given by [17]:

$$k = \frac{\omega b}{U} \tag{26}$$

By substituting Eq.(24) and Eq.(26) into the equation of motion Eq.(23) yields;

$$[K_w]\{\bar{q}_3\} - \omega^2\left([M_w] + [\bar{A}]\right)\{\bar{q}_3\} = 0 \tag{27}$$

where $[\bar{A}]$ represents the aerodynamic matrix:

$$[\bar{A}] = \rho\frac{b^2}{2k^2}[a_{3R}][Ar_R] \tag{28}$$

The flutter analysis can be performed using the U-g method [17]. The structural damping coefficient (g) is introduced in the equations of motion which representing the amount of damping that must be added to the

ISSN: 2277-3754
ISO 9001:2008 Certified
International Journal of Engineering and Innovative Technology (IJEIT)
Volume 4, Issue 2, August 2014

structure to attain neutral stability (flutter) at the given velocity [1]. Negative values of structural damping (g) indicate that the structure is stable, while positive values indicate instability of the structure. Flutter occurs when the structural damping coefficient (g) equals zero. From Eq.(27) the eigenvalue problem can be written as:

$$\begin{aligned}&\left((1+ig)[K_w]-\omega^2\left([M_w]+[\bar{A}]\right)\right)\{\bar{q}_3\}=0\\&\left(Z\,[K_w]-[\bar{B}]\right)\{\bar{q}_3\}=0\end{aligned} \tag{29}$$

where

$$[\bar{B}]=[M_w]+[\bar{A}] \tag{30}$$

and

$$Z=\frac{(1+ig)}{\omega^2} \tag{31}$$

For a given value of reduced frequency k the complex aerodynamic matrix $[\bar{A}]$ is evaluated using Eq.(28), and the matrices $[\bar{A}]$ with $[M_w]$ and $[K_w]$ are placed into Eq.(29) Which is solved for the complex eigenvalues Z. From these eigenvalues and the given k, the frequency (ω), the structural damping coefficient (g), and the corresponding speed (U) are determined as flows:

$$\omega=\sqrt{\frac{1}{Z\,(\mathrm{Re})}},\qquad g=\frac{Z\,(\mathrm{Im})}{Z\,(\mathrm{Re})},\qquad U=\frac{\omega b}{k} \tag{32}$$

In Figure 2, U characterizes the flutter speed and frequencies of the wing. The value of the parameter ω at g=0 represents the flutter frequency [1].

V. DIVERGENCE

The divergence speed (U_D) can be calculated directly by neglecting the mass matrix $[M_w]$ in Eq.(27) and rearranging equations as the following form:

$$\left([\bar{A}_{stat}]-\lambda[K_w]\right)\{\bar{q}_3\}=0 \tag{33}$$

where the static aerodynamic matrix $[\bar{A}_{stat}]$ has all real coefficients, and is represented by:

$$[\bar{A}_{stat}]=\lim_{k\to 0}\frac{1}{2}\rho[a_{3R}][Ar_R] \tag{34}$$

and the eigenvalue λ is given by:

$$\lambda=\frac{1}{U_D^2} \tag{35}$$

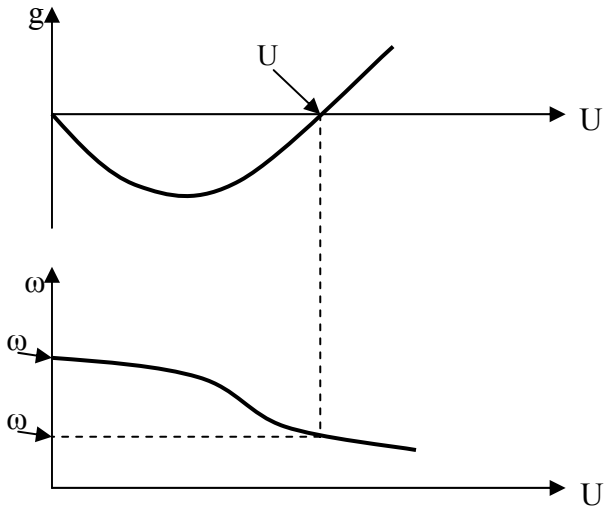

Fig 2. U-g and U-ω curves to find flutter speed and frequency (U_f, ω_f) [1].

The largest positive eigenvalue λ gives the lowest divergence speed U_D. Figure 3 of g and ω vs. U characterizes the divergence speed (U_D) of the wing.

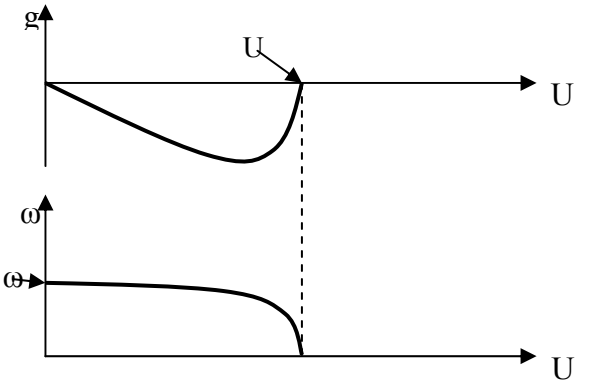

Fig 3. U-g and U-ω curves to find divergence speed (U_D) [1].

VI. NUMERICAL RESULTS AND DISCUSSION

The aerodynamic and aero elastic theories are first verified then a parametric study is performed. A MATLAB code for the used doublet point method is developed and verified on a rectangular wing for steady and unsteady flow. The pressure distribution, lift and moment coefficients are calculated, and then the flutter and divergence performance of a rectangular composite plate is also calculated. The obtained results are compared with the available published data. Finally the effect of composite fiber orientation on natural frequency, flutter and divergence speeds is computed.

ISSN: 2277-3754
ISO 9001:2008 Certified
International Journal of Engineering and Innovative Technology (IJEIT)
Volume 4, Issue 2, August 2014

A. Aerodynamics characteristics of the wing in steady flow

A rectangular wing of aspect ratio (AR=2) in steady state flow $(k \to 0)$ is used in this study. The wing rotates around its mid-chord with angle of attack (α). A three dimensional (3-D) pressure distribution of rectangular wing with equal number of elements in x and y directions are calculated and shown in Figure 4. The chord-wise pressure coefficient distribution of the wing at station y=0.2 is shown in Figure 5 for three different numbers of elements N_x. The lift coefficient distribution is shown in Figure 6. It is calculated by the steps mentioned in Appendix B with fixed chord wise number of elements.

B. Aerodynamics characteristics of the wing in unsteady flow

A rectangular wing of aspect ratio (AR=2) is used in the validation of the wing in unsteady flow. The wing oscillates in pitching around its mid-chord with angle of attack (α). The real and imaginary parts of the pressure distribution are shown in Figure 7 and Figure 8, respectively. Also the real and imaginary parts of the span-wise distributions of the lift coefficient slope c_{l_α} are shown in Figure 9 and Figure 10, respectively. The chord wise distributions of the real and imaginary parts of the pressure coefficient c_{P_α} at the tip and root of the considered wing are shown in Figure 11 and Figure 12, respectively. Figure 13 shows the magnitude of the complex lift and moment coefficients C_L and C_M verses the reduced frequency (k). Figure 14 presents the phase of the complex lift and moment coefficients C_L and C_M verses the reduced frequency (k). The lift and moment coefficients are calculated as given in Appendix B. All the presented results are compared with the published data given by reference [14] and found reasonable.

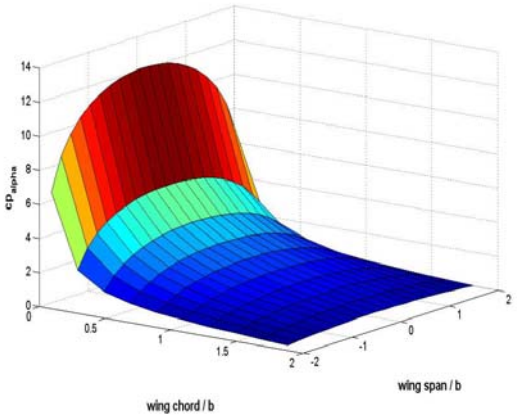

Fig 4. 3-D pressure distribution of rectangular wing (AR=2, k=0, M=0, N_x=10, N_y=10).

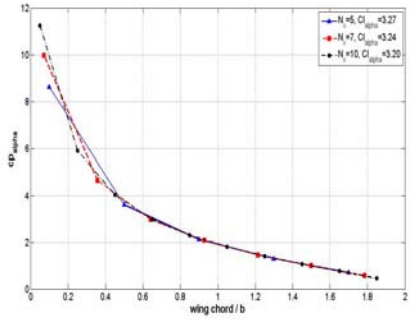

Fig 5. Chord wise pressure coefficient slope distribution of the wing at station y=0.2 (AR=2, k=0, M=0, N_y=10).

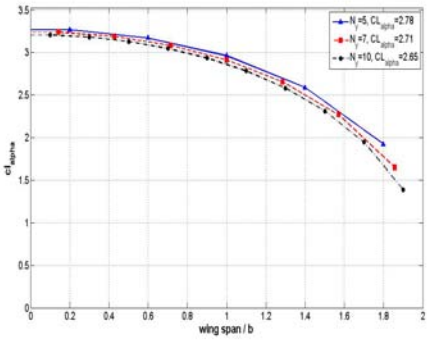

Fig 6. Span wise lift coefficient slope distribution of the wing (AR=2, k=0, M=0, N_y=10).

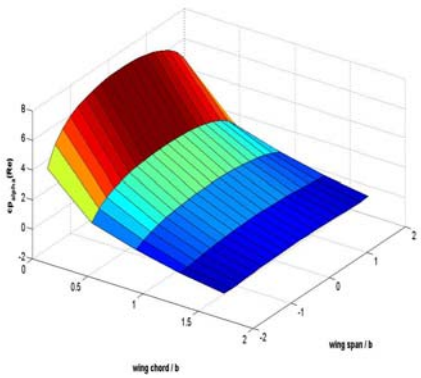

Fig 7. Real part of the pressure distribution of rectangular wing oscillates in pitching motion (AR=2, k=1, M=0, N_x=5, N_y=10).

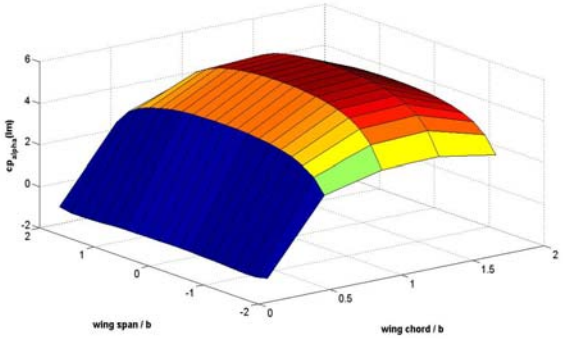

Fig 8. Imaginary part of the pressure distribution of rectangular wing oscillates in pitching motion (AR=2, k=1, M=0, N_x=5, N_y=10).

ISSN: 2277-3754
ISO 9001:2008 Certified
International Journal of Engineering and Innovative Technology (IJEIT)
Volume 4, Issue 2, August 2014

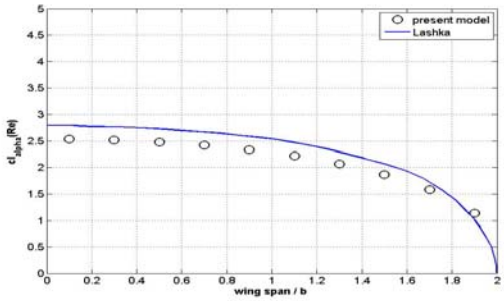

Fig 9. Real part of the lift coefficient slope distribution $C_{l_\alpha R}$ of a rectangular wing oscillates in pitching motion (AR=2, k=1, M=0, N_x=5, N_y=10).

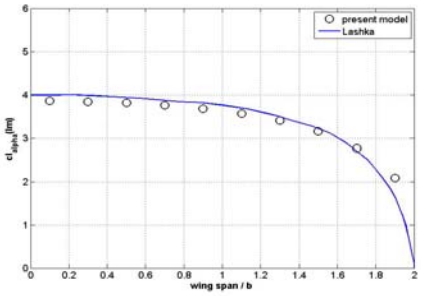

Fig 10. Imaginary part of the lift coefficient slope distribution $C_{l_\alpha I}$ of rectangular wing oscillates in pitching motion (AR=2, k=1, M=0, N_x=5, N_y=10).

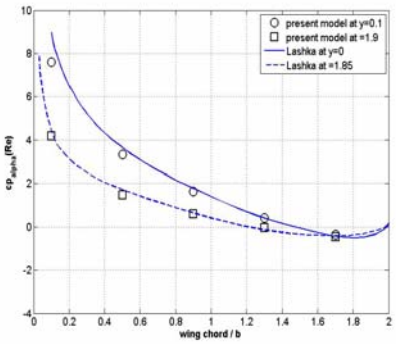

Fig 11. Real part of the chord wise pressure coefficient distribution $C_{P_\alpha R}$ at the tip and root of a rectangular wing oscillates in pitching motion (AR=2, k=1, M=0, N_x=5, N_y=10).

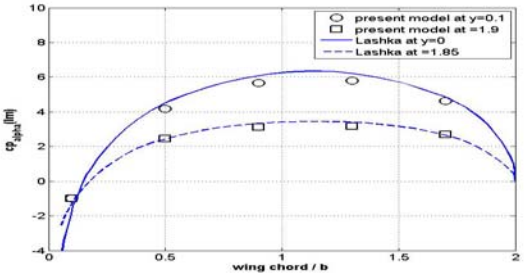

Fig 12. Imaginary part of the chord wise pressure coefficient distribution $C_{P_\alpha I}$ of rectangular wing oscillates in pitching motion (AR=2, k=1, M=0, N_x=5, N_y=10).

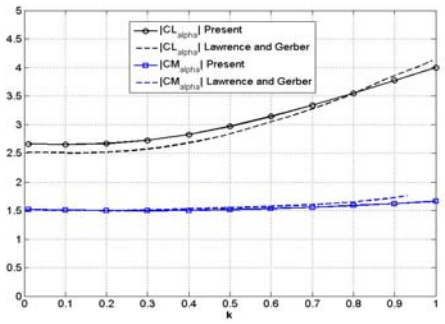

Fig 13. The complex lift and moment coefficients C_L and C_M of rectangular wing oscillates in pitching motion vs. the reduced frequency.

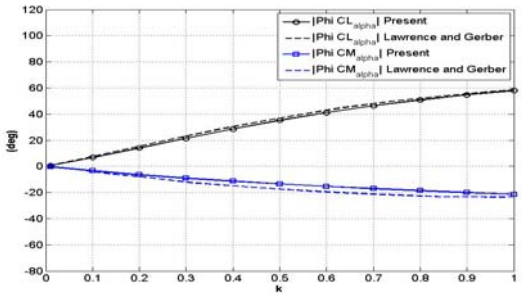

Fig 14. The phase of the complex lift and moment coefficients C_L and C_M of a rectangular wing oscillates in pitching motion vs. the reduced frequency.

C. Aero elastic performance of the Composite Plate wing

A rectangular cantilevered composite plate is considered as a half-span representation of an aircraft wing. The plate has a length of L=12 in (0.3048 m) and a width of 2b=3 in (0.0762 m), and a thickness of t=0.804×10^{-3} m. A six layers of unidirectional graphite/epoxy tape with stacking sequence $[0_2/90]_s$, $[\pm45/0]_s$, $[+45_2/0]_s$, $[-45_2/0]_s$, $[+30_2/0]_s$, $[-30_2/0]_s$ are used.

The material constants of the individual layers are listed in Table 1 [1].

Table 1. Engineering constants of the unidirectional graphite/epoxy tape [1].

E_{11} [GPa]	$E_{22}=E_{33}$ [GPa]	G_{12} [GPa]	ν_{21}	Ply thickness t_p [mm]	Density ρ [kg/m^3]
98	7.9	5.6	0.28	0.134	1520

The obtained natural frequencies are shown in Table 2 using 5-term Rayleigh-Ritz method have generally good agreement with published experimental data and analytical natural frequencies [1].

ISSN: 2277-3754
ISO 9001:2008 Certified
International Journal of Engineering and Innovative Technology (IJEIT)
Volume 4, Issue 2, August 2014

Table 2. Natural frequencies of laminated composite plate.

Laminate	Vibration mode	Meas. Freq., [Hz], [1]	Ref [1]		Present model	
			freq., [Hz]	Δ %	freq., [Hz],	Δ %
$[0_2/90]_s$	1B	11.1	10.7	-3.6	11.06	-0.33
	2B	69	67	-2.9	70.09	1.58
	1T	42	39	-7.14	39.75	5.36
$[\pm 45/0]_s$	1B	6.1	5.7	-6.56	5.986	1.87
	2B	38	37	-2.63	36.76	-3.27
	1T	77	69	-10.4	71.71	-6.87
$[+45_2/0]_s$ $[-45_2/0]_s$	1B	4.8	4.6	-4.17	4.004	-16.6
	2B	30	32	6.667	26.76	-10.8
	1T	51	55	7.843	56.24	10.3
$[+30_2/0]_s$ $[-30_2/0]_s$	1B	6	6	0	6.118	1.97
	2B	36	41	13.89	37.45	4.03
	1T	58	60	3.448	62.98	8.59

Δ is the percent of the error.

The U-g and U-ω diagrams for the proposed plates are shown in Figure 15 to Figure 18. Using 9-term Rayleigh-Ritz method and 6×8 aerodynamic Doublet Points, flutter speeds (U_f) and flutter frequencies (ω_f) are listed in Table 3. Results are compared to experimental data [1], analytical results calculated using 5-term Rayleigh-Ritz method, applying strip theory for the aerodynamic modeling [1]. For further verification two extra finite element models are considered, 3×12 FE, using Doublet Lattice method for aerodynamic model [2], and 2×6 FE using 6×8 Doublet Point method [3]. The results are accurate for $[+45_2/0]_s$ and $[+30_2/0]_s$ plates, while for other stacking sequences flutter speeds are differ. It is noticeable from Figure 15 to Figure 18 that the bending mode is responsible for the flutter phenomenon in the plates of $[+45_2/0]_s$ and $[+30_2/0]_s$ stacking sequences, while the torsional mode is responsible for the flutter phenomenon in the other plates. The prediction of the

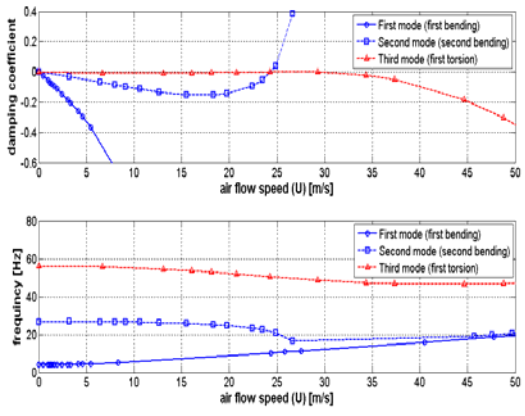

Fig 15. The U-g curve and U-frequency curve for a $[+45/0]_s$ plate wing.

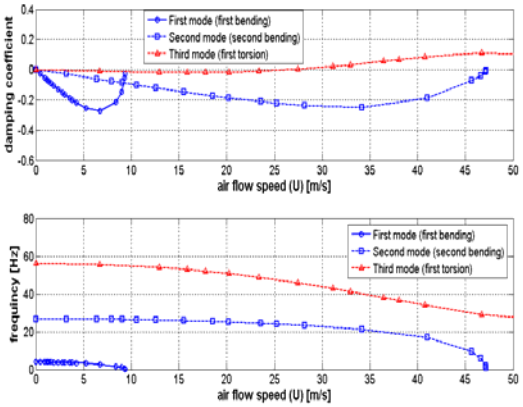

Fig 16. The U-g curve and U-frequency curve for a $[-45/0]_s$ plate wing.

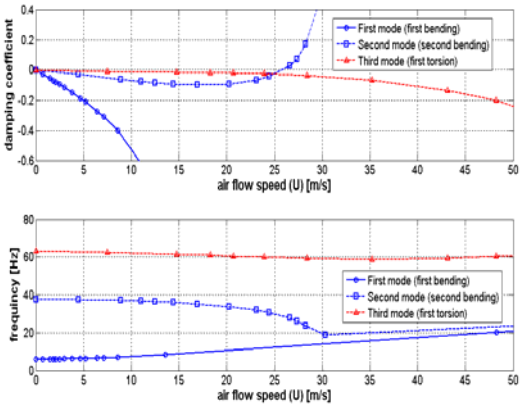

Fig 17. The U-g curve and U-frequency curve for a $[+30/0]_s$ plate wing.

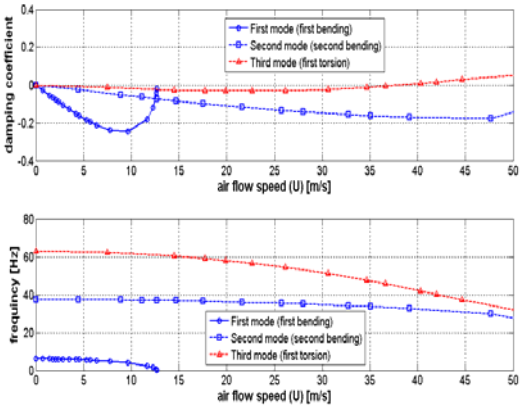

Fig 18. The U-g curve and U-frequency curve for a $[-30/0]_s$ plate wing.

divergence speeds (U_D) are listed in Table 4.. The same theories used in flutter validation. The comparison shows a good agreement in all stacking sequences.

ISSN: 2277-3754
ISO 9001:2008 Certified
International Journal of Engineering and Innovative Technology (IJEIT)
Volume 4, Issue 2, August 2014

Table 3. Flutter speed [m/s] and flutter frequency [Hz] of laminated composite plate.

	$[+45_2/0]_s$		$[-45_2/0]_s$		$[+30_2/0]_s$		$[-30_2/0]_s$	
	U_f	ω_f	U_f	ω_f	U_f	ω_f	U_f	ω_f
Experimental,[1]	28	24	div.	div.	27	28	div.	div.
Present model Rayleigh-Ritz (9 terms), Aero (Doublet Point) 6×8	23.6	21	div. 25.1	div. 48.1	25.8	28.9	div. 37.7	div. 45.2
Rayleigh-Ritz 5 terms, Aero (strip theory), [1]	27.8	28	27.8	27	27.8	31	30	29
FE 3×12, Aero (Doublet Lattice),[2]	-	-	-	-	24.9	26.4	-	-
FE 2×6, Aero Doublet Point 6×8,[3]	27.6	23.9	-	-	27.2	28	-	-

Table 4. Divergence speed of laminated composite plate.

	$[0_2/90]_s$	$[\pm 45/0]_s$	$[+45_2/0]_s$	$[-45_2/0]_s$	$[+30_2/0]_s$	$[-30_2/0]_s$
Experimental,[1]	flutter	>32	flutter	12.5	flutter	11.7
Present model Rayleigh-Ritz (9 terms), Aero (Doublet Point) 6×8	29.13	No div.	No div.	9.125	No div.	12.33
Rayleigh-Ritz (5 terms), Aero (strip theory), [1]	22.3	infinite	infinite	9.9	infinite	10.2
Rayleigh-Ritz (5 terms), Aero (modified strip theory), [1]	25	No div.	No div.	11.1	No div.	11.5

D. Effect of the plate fiber orientation angle on Flutter and Divergence

A proposed plate is considered as a half-span of an aircraft wing. The plate has an aspect ratio (AR=4), width (2b=1 m), and total thickness (t=0.016 m). The material properties of the proposed plate are given in Table 5, [2].

Table 5. Material properties of the composite plate [2].

E_{11} [GPa]	$E_{22}=E_{33}$ [GPa]	G_{12} [GPa]	ν_{21}	Ply thickness t_p [mm]	Density ρ [kg/m^3]
32	4	1.6	0.25	0.134	1500

The composite fiber angle is varied in the range (-90° to 90°). Flutter and divergence speeds (U_f, U_D) and the flutter and natural frequencies (ω_f, ω_n) are calculated and plotted as normalized values in Figure 19 and Figure 20, respectively. The obtained results have good correlation with those in reference [2]. It is clear that positive fiber angles produce divergence-free wings, but the wing flutter speeds are small relative to negative fiber orientation angle. Therefore it is difficult to obtain composite tailoring that simultaneously achieves high-flutter and high-divergence boundaries.

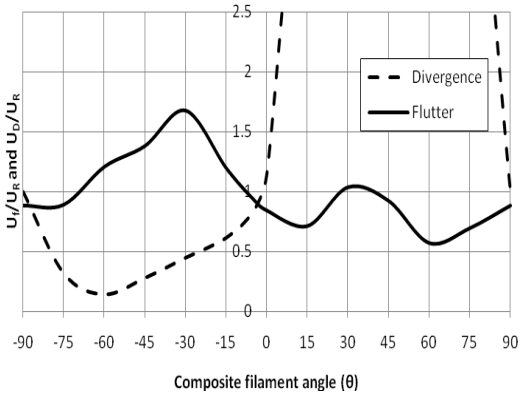

Fig 19. Flutter and divergence speeds (U_f, U_D) normalized with respect to U_R=44.67 m/s (U_D at θ=90°).

ISSN: 2277-3754
ISO 9001:2008 Certified
International Journal of Engineering and Innovative Technology (IJEIT)
Volume 4, Issue 2, August 2014

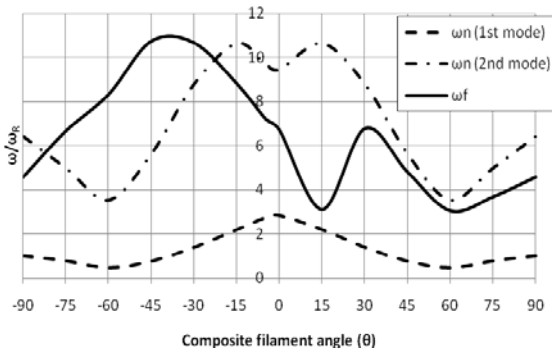

Fig 20. Flutter and natural frequencies (ω_f, ω_n) normalized with respect to ω_R=1.665 rad/sec (1st natural frequency at θ=90°).

VIII .CONCLUSION

An analytical investigation was proposed to determine the flutter and divergence behavior of unswept rectangular wings simulated by cantilevered composite plates using energy formulation and unsteady incompressible two-dimensional aerodynamic theory. Doublet point method was used to solve the subsonic unsteady flow over a rectangular wing to get the pressure and aerodynamic lift distribution. The modified higher order plate theory was used with the aerodynamic model to determine aero elastic performance. Flutter and divergence velocities are obtained using the U-g method and they compared to the published analytical, finite element and wind tunnel test results and found reasonable. It is concluded that positive fiber angles produce divergence-free wings, but the flutter speeds are small relative to negative fiber angle wings. Therefore it is difficult to obtain composite tailoring that simultaneously achieves high-flutter and high-divergence boundaries.

REFERENCES

[1] S. J. Hollowell and J. Dugundji "Aeroelastic flutter and divergence stiffness coupled, graphite/epoxy cantilevered plates" Journal of Aircraft, vol. 21, No. 1, pp. 69-76,1984.

[2] K. J. Lin, P. J. Lu, and J. Q. Tarn "Flutter Analysis of cantilever composite plate in subsonic flow" AIAA Journal, vol. 27, pp. 1102-1109, 1989.

[3] K. N. Koo and I. Lee "Aeroelastic behavior of a composite plate wing with structural damping" Computers & Structures, vol. 50, No. 2, pp. 167-176, 1994.

[4] W. G. Abdelrahmen "Static and dynamic behaviour of composite swept wings" Master thesis, Dept. of Aerospace, Faculty of engineering, Cairo univeristy, Egypt.

[5] P. Dunn and J. Dugundji "Nonlinear stall flutter and divergince analysis of cantilever graphite/epoxy wings" AIAA Journal, vol. 30, No. 1, pp. 153-162, January 1992.

[6] E. Livne and W.-L. Li "Aeroservoelastic aspects of wing/control surface planform shape optimization" AIAA Journal, vol. 33, No. 2, pp. 302-311, 1995.

[7] P.-J. Lu and L.-J. Huang "Flutter suppression of thin airfoils using active acoustic excitations" AIAA Journal, vol. 30, No. 12, pp. 2873-2881, 1992.

[8] H. G. Kussner "General Airfoil Theory," NACA TM 979, 1941.

[9] C. E. Watkins, D. S. Woolston, and H. J. Cunningham"A systematic Kernel function procedure for determining aerodynamic forces on oscillating or steady finite wings at subsonic speeds" NASA TR R-48, 1959.

[10] W. S. Rowe, M. C. Redman, F. E. Ehlers, and J. D. Sebastian "Prediction of unsteady aerodynamic loadings caused by leading edge and trailing edge control surface motion in subsonic compressible flow- Analysis and results" NASA CR-2543, 1975.

[11] E. Albano and W. P. Rodden, "A doublet lattice method for calculating lift distribution on oscillating surfaces in subsonic flows" AIAA Journal, vol. 7, pp. 279-285, 1969.

[12] M. Blair "A compilation of the mathimatics leading to the doublet lattice method" Wright Laboratory, WL-TR-92-3028, March 1992.

[13] W. P. Rodden, Paul F. Taylor, and Samuel C. McIntosh "Further refinement of the subsonic doublet-lattice method" Journal of Aircraft, vol. 35, No.5, pp. 720-727,1998.

[14] T. Ueda and E. H. Dowell "A new solution method for lifting surfaces in subsonic flow" AIAA Journal, vol. 20, pp. 348-355, 1982.

[15] M. Kassem Abbas, M. Adnan Elshafei, and H. M. Negm "Modeling and Analysis of Laminated Composite Plate Using Modified Higher Order Shear Deformation Theory" presented at the 15th international conference on aerospace sience & aviation technology, ASAT-15, 2013.

[16] E. H. Dowell, Sijthoff and Noordhoff, and Alphen aaan Rijn" A Modern Course in Aeroelasticity" The Netherlands, 1978.

[17] R. L. Bisplinghoff, Holt Ashley, and Robrt L. Halfman" Aeroelasticity". Mineola, New York: Dover Publications, inc., 1996.

Appendix A

Parameters used in the Eq.(6) [14]:

$$x_0 = x - \zeta \qquad y_0 = y - \eta \qquad r = |y_0|$$

$$R = \sqrt{x_0^2 + \beta^2 r^2} \qquad X = \frac{(x_0 - MR)}{\beta^2} \qquad \beta = \sqrt{1 - M^2} \tag{A-1}$$

The function $B(k, r, X)$ in the Kernel function, Eq.(6), is represented as:

$$B(k, r, X) = \int_{-\infty}^{X} \frac{e^{ikv}}{(v^2 + r^2)^{3/2}} dv \tag{A-2}$$

ISSN: 2277-3754
ISO 9001:2008 Certified
International Journal of Engineering and Innovative Technology (IJEIT)
Volume 4, Issue 2, August 2014

The function $B(k,r,X)$ can be separated into two real functions as:

$$B(k,r,X) = B_R(k,r,X) + iB_I(k,r,X) \quad \text{(A-3)}$$

Values of these functions can be obtained as follows [18]:

$$B_R(k,r,X) = \int_{-\infty}^{X} \frac{\cos(kv)}{(v^2+r^2)^{3/2}}dv, \quad B_I(k,r,X) = \int_{-\infty}^{X} \frac{\sin(kv)}{(v^2+r^2)^{3/2}}dv \quad \text{(A-4)}$$

These functions can be expressed as:

$$B_R(k,r,X) = \sum_{n=0}^{\infty}(-1)^n U_{2n} - \frac{k^2}{2}\sum_{n=0}^{\infty}\frac{(kr/2)^{2n}}{(n+1)(n!)^2} \times \left\{\sum_{m=1}^{n}\frac{1}{m} + \frac{1}{2(n+1)} - \gamma - \ln\frac{k}{2}\right\} \quad \text{(A-5)}$$

$$B_I(k,r,X) = \sum_{n=0}^{\infty}(-1)^n U_{2n+1} + \frac{\pi}{4}k^2\sum_{n=0}^{\infty}\frac{(kr/2)^{2n}}{(n+1)(n!)^2} \quad \text{(A-6)}$$

where the term U_n is a function of X, and can be calculated with the aid of the recurrence formula:

$$U_n = \frac{k}{(n-2)n!}\frac{(kX)^{n-1}}{\sqrt{X^2+r^2}} - \frac{(kr)^2}{n(n-2)}U_{n-2} \qquad (n \geq 3) \quad \text{(A-7)}$$

The initial terms of the recurrence formula Eq.(A-7) are given by:

$$U_0 = \frac{1}{\sqrt{X^2+r^2}\left(\sqrt{X^2+r^2}-X\right)}$$
$$U_1 = \frac{-k}{\sqrt{X^2+r^2}} \quad \text{(A-8)}$$
$$U_2 = -\frac{k^2}{2}\left[\frac{X}{\sqrt{X^2+r^2}} + \ln\left(\sqrt{X^2+r^2}-X\right)\right]$$

when an up wash point is downstream of a doublet point the value of the function B_R which is evaluated by [14]:

$$B_R(k,r,X) \to B_R(k,r,-X) - \frac{\pi^2}{6\sigma_j^2} + k^2\left(\ln\frac{k\sigma_j}{2} + \gamma - \frac{3}{2}\right) \quad (r<\sigma_j, X>0) \quad \text{(A-9)}$$

where γ is the Euler's constant $\gamma \approx 0.5772$.

Appendix B

The complex lift and moment coefficients can be calculated by taking the following chord wise summation at span station $y = y_j$ [14],

$$C_l(y_j) = \frac{\sum_i^{N_x} c_{p_i}\Delta_i}{\sum_i^{N_x}\Delta_i}, C_m(y_j) = \frac{\sum_i^{N_x} c_{p_i}\Delta_i(x_m - x_i)}{\sum_i^{N_x}\Delta_i} \quad \text{(B-1)}$$

The total lift and moment coefficients of the wing can be calculated by taking the following span wise summations,

$$C_L = \frac{\sum_j^{N_y}\left[C_l(y_j)\sum_i^{N_x}\Delta_i\right]}{S}, C_M = \frac{\sum_j^{N_y}\left[C_m(y_j)\sum_i^{N_x}\Delta_i\right]}{S} \quad \text{(B-2)}$$

where S is a total wing area and x_m the location of the axis around which the moment force is calculated.